PET Imaging Physics and Instrumentation

Christopher J Thompson, D.Sc. FCCPM
Montreal Neurological Institute
Christopher.Thompson.McGill.Ca

This article deals with how PET images are formed, and the equipment needed to form them. The reader will be introduced to the different types of PET system geometries, and the advantages and disadvantages of each system. Emission scans are compared and contrasted to transmission scans, and the concept of attenuation correction is introduced. The issues pertaining to image quality are discussed, in order to understand what makes a good PET image, and identify some of the causes of poor quality PET images. Different types of PET image presentation (slice-by-slice and whole body scans) are discussed at the end of the chapter.

## 1 Formation of PET Images

This section deals with the basic principles of PET imaging. A basic understanding of what produces PET images is important in order to appreciate both the advantages of PET imaging and its limitations. Why are PET images "noisier" than those from an X-ray CT scanner? Why is the spatial resolution of PET lower than that of MRI? Why are PET images considered to be "functional" as opposed to "anatomical"? What has been done, and what can still be done to improve PET image quality?

### 1.1 Radioactive decay by positron emission

Unlike other instruments used in Nuclear Medicine, dedicated PET scanners can only detect isotopes which decay by positron emission. The only exception to this is $^{137}$Cs which is used in some recent PET scanners for doing transmission scans as discussed later. The most common isotopes, (and their properties) used in clinical practise are given in Table I.

A schematic diagram showing what happens after positron decay is shown in Figure 1. When an isotope emits a positron, the mass difference between the parent and daughter isotopes becomes energy which is shared unevenly between the daughter nucleus and the positron. The positron is therefore ejected with enough kinetic energy to travel some distance from the parent nucleus. It must lose this energy before combining with an electron and eventually annihilating. It does this by making collisions in the medium in which it is travelling. Thus an important part of this table is the "mean positron range", which imposes a lower limit on the spatial resolution of any PET system. The mean range values in the table are given for water. The values are smaller in bones, but much larger in the lungs, and several metres in air! The blurring associated with this process is known as positron range blurring, and it depends on the isotope and the medium in which the radioactive decay occurs.

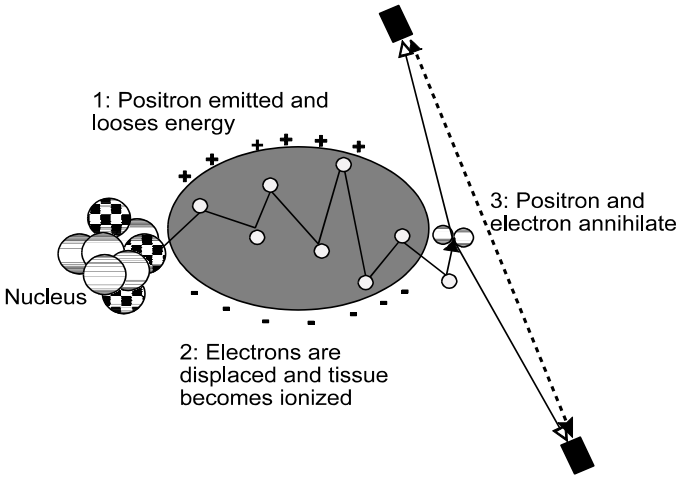


**Figure 1** A nucleus undergoes positron decay. Subsequent annihilation of positron and electron produces two γ rays which travel away from the site at almost 180° and are then detected.

| Isotope | Half-life (units) | Positron range (mm) | Production | Applications |
|---|---|---|---|---|
| $^{11}C$ | 20.4 (min) | 1.7 | Cyclotron | Various |
| $^{13}N$ | 10.0 (min) | 2.0 | Cyclotron | Cardiac blood flow |
| $^{15}O$ | 2.07 (min) | 2.7 | Cyclotron | Cerebral blood flow |
| $^{18}F$ | 110 (min) | 1.4 | Cyclotron | Glucose metabolism |
| $^{82}Rb$ | 1.2 (min) | 4.0 | Generator | Cardiac blood flow |
| $^{68}Ge$ | 260 (day) | 3.0 | Purchase | Transmission scan |
| $^{137}Cs$ | 5 (year) | NA | Purchase | Transmission scan |

**Table I** Properties of isotopes commonly used with PET

### 1.2 Annihilation of positron and electron

The fundamental signal in PET results from the mutual annihilation of the positron and an electron. This results in the production of two γ rays each having the energy corresponding to the mass of an electron (ie 511 keV), and a neutrino.

### 1.3 Two γ-rays produced

The two γ-rays are emitted at exactly 180° apart with respect to the electron-positron pair as shown in Figure 1. However, since the both the electron and positron were certainly moving when this happened, the apparent angle is not quite 180° but has a random variation of about 0.5°. Since this angle is unpredictable, and cannot be measured, PET scanner software must assume that the angle was 180°, and this causes additional blurring of the image. The magnitude of this error depends on the distance separating the two detectors, so can be reduced in scanners designed for brain-only studies, or in small animal PET scanners. The blurring associated with this process is known as non-collinearity blurring, and it depends on the energy of the electron involved in the annihilation, and the separation of the detectors.

### 1.4 Both γ-rays may escape patient section and be detected

Both the γ-rays must escape the patient section in order to be detected. If neither is scattered then the line joining the two detectors will intersect the point of annihilation (apart from the error due to non-collinearity referred to in the previous section). Only unscattered γ-ray pairs contribute useful information to the precess of image formation. Unscattered γ-ray pairs are referred as "true" counts, to distinguish them from "scattered counts".

### 1.5 Coincident detection of γ rays constitutes one "count"

The near-simultaneous detection of a pair of γ-rays represents one event or count in the image. The line joining the two detectors is referred to as a line of response or LOR (the dashed line in Figure 1). Images are formed from millions of these counts. Even though both γ-rays are emitted at the same time,

they may not be detected at exactly the same time. The point of annihilation is not confined to the centre of the image field, in fact, during transmission scans, it is beyond the edge for the image field. Since they γ-rays travel at the speed of light (~30 cm/nsec) the detection times can be different by over 2 nsec for a typical PET scanner with an aperture of 60 cm. For this reason, and also due to errors in timing, a short time window is set during which pairs of γ-rays are considered to be "in-coincidence". This window is typically in the range of 8-16 nsec, for body scanners with relatively "slow" scintillation crystals.

It is possible, and at high count-rates quite likely, that two γ-rays which did not originate in the same annihilation can be detected within this time window. Such events are referred to as "random counts".

**1.6 Counts recorded in sinogram for image reconstruction**

During a PET scan, all of these counts must be collected and stored. An array of memory is allocated for this purpose, and before the scan starts, all the memory locations are set to "zero". During the scan memory locations associated with each line of response are incremented, so that each event is actually "counted" as it comes in. Modern PET scanners have thousands of detectors, and this results in millions of LORs. The storage matrix representing all the LORs can be made more compact by recognizing symmetries in PET scanners, and by combining counts from very close LORs into one memory location.

The memory arrays used for data storage, are often referred to as "sinograms" from the pattern associated with counting events from an off-centre point source in one of these arrays. The horizontal coordinate is derived from the difference of the detector numbers in a ring scanner, and the vertical coordinate is the average of the detector numbers. This format of data storage is both compact, and in a suitable form for direct use by the image reconstruction program. Figures 2 and 3 illustrate the relationship between the detectors on the circumference of a circle and a sinogram. Consider that there is activity in only one location in the scanner's field of view. The point of annihilation is represented by A in figure 2, and is a distance, d, from the centre, and the two γ-rays are detected by crystals at positions A and B. The chord, PQ, is a distance, s, from the centre of the ring. The line from A to the origin makes and angle, α, and the line from the chord AB to the centre makes an angle β or (P+Q)/2. All γ-ray pairs

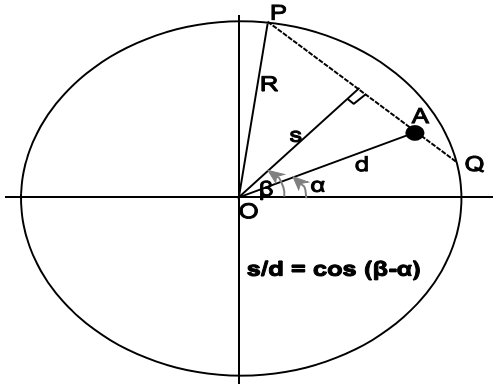


**Figure 2** A is the point of annihilation, P and Q are the detectors involved. The distance from A to the origin is represented by d. The distance from the LOR to the origin is represented by s. The angle α is measured to the line joining the point of annihilation to the origin, and β is measured to the normal of the LOR.

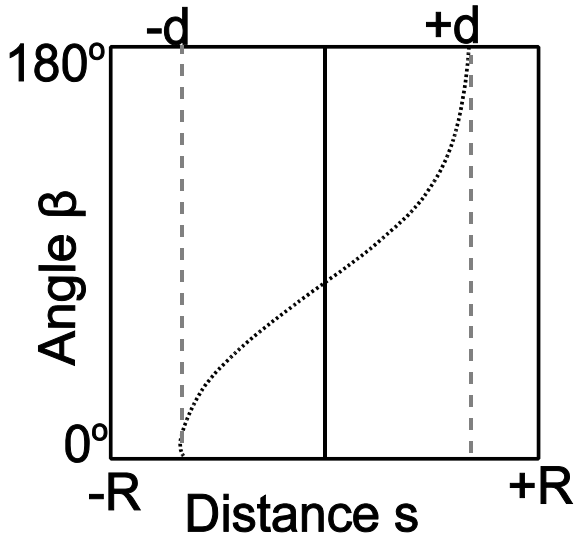


**Figure 3** Sinogram for point source at distance, d, from the origin of PET detector ring of radius, R, and the angle β is the average angle of the two detectors defining the LOR.

emanating from the source pass through A, but will interact with other detectors, so that while d and α are constant for this point, β and s will vary. The relationship is given by:

$$s = d\cos(\beta - \alpha) \quad (1)$$

and this is depicted in figure 3. So this one point source will cause counts to be accumulated along the cosine curve represented by the dotted line in figure 3. The points in one horizontal row of a sinogram make up a "projection". Each projection represents the counts acquired by a set of detector-pairs which are all at the same angle, or whose LORs are parallel to one another. Figure 4 shows how a projection at the angle $\beta = (P_n + Q_n)/2$ has inputs from detectors which lie on contiguous parallel chords.

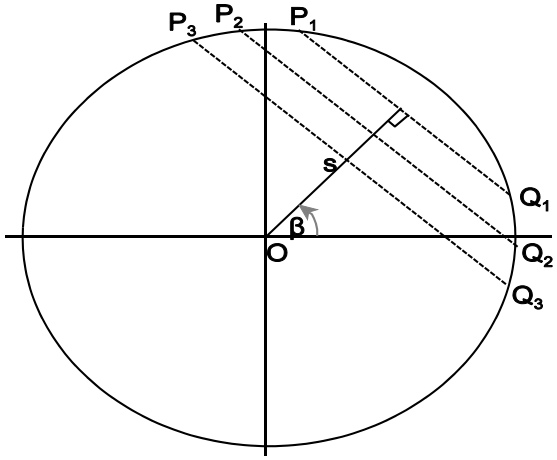


**Figure 4** These three LORs are parallel and at an angle β = (P+Q)/2. If the P's and Q's are contiguous detectors, these LORs are represented in the sinogram by contiguous horizontal samples on the line corresponding to the angle (P+Q)/2.

## 2 Components of a PET system

A modern PET scanner is a highly sophisticated piece of equipment comprising a patient handling system, data collection system, image reconstruction, display and archival systems. While the patient handling and image display components are the most conspicuous, the other systems play a vital role in image quality, and patient throughput.

This section deals with detection of γ-rays and processing of counts as they impact of image quality. The other components are only discussed with respect to their impact on these issues. Throughout this section we will assume a PET ring geometry, as other detector geometries are discussed in the next section.

### 2.1 Collimators

Collimators in PET scanners are positioned to confine the radiation detected to that which originates within the scanning field of view. Some early PET scanners[1, 2] had one ring of detectors, and thick rings of lead where placed in front of, and behind the plane of these detectors to reduce the probability of detecting γ-rays from outside the slice being imaged. With the introduction of multi-slice scanners, the thick lead rings were maintained to define the external axial field of view, and thin lead or tungsten rings (1-5 mm thick) usually referred to as "septa" were employed to define the individual imaging planes.

Most present commercial PET scanners now have these septa configured so that they can be positioned to define the slices during 2D PET studies, but they can be retracted during 3D scans (see below).

The collimators in PET are very different that those on a gamma camera. The common parallel-hole collimator on a gamma camera restricts the detection of γ-rays to those which are almost normal to the crystal face. A high resolution gamma camera collimator rejects almost all of the radiation emitted from a patient in the direction of the gamma camera, since most of it does not approach the crystal almost perpendicular to the surface.

On the other hand, even in the 2D configuration, each element of a PET detector has a very wide

field of view. The principle of coincidence detection provides an "electronic collimation" of the counts. One could think of the detector at one end of a line of response as identifying the point of detection and the other detector providing the angle of incidence.

The concept of electronic collimation is what makes PET imaging much more efficient (in terms of detected counts per injected dose) than other Nuclear Medicine procedures. However the 99% of the radiation absorbed by the gamma camera's collimator goes undetected. The equivalent amount of single γ-rays are detected by the PET system's detectors, but rejected by the coincidence circuit. While the perforated lead gamma camera collimator is a passive system, each γ-ray must be detected and paired with another to produce one count. In practise about 99% of the γ-rays detected by the crystals are rejected by the coincidence circuit. Since each detector can correctly identify only one γ-ray at a time, a great deal of time is spent processing γ-rays which will never correspond to a coincident count. This time lost is referred to as "dead-time" and is the major limitation for image quality when doing PET studies with short lived isotopes.

### 2.2 Detectors

The detectors in a PET scanner perform much more than those of a gamma camera. As was mentioned in the previous section they detect mostly single γ-rays, which are later discarded, but are required to be ready to detect the γ-ray pairs which are in coincidence. In order to do this successfully, the detectors in dedicated PET are much smaller than those of a gamma camera. A lot of small independent detectors result in lower "dead-time" losses.

Most isotopes used in Nuclear Medicine have relatively low energies (eg $^{99m}$Tc at 133 keV), and are detected with a very high efficiency by the relatively thin (6 - 10 mm) NaI(Tl) crystal of a gamma camera. PET detectors are required to detect the 511 keV γ-rays from positron annihilation, and so detectors with much higher stopping power are required.

In order to record a useful "count", both detectors must each detect their γ-ray, so that in PET the probability of detecting a count depends on the square of the single detector's efficiency. For this reason, PET detectors are also made thicker than those in a gamma camera. The crystals in gamma cameras are made as thin as possible (while allowing for adequate efficiency) to improve their spatial resolution. So using very thick crystals to provide adequate efficiency for PET imaging, while providing good spatial resolution, appears to be a paradox.

In order to satisfy these seemingly contradictory requirements, early PET systems [1, 2] used single crystals coupled to individual photo-multipliers. This was mainly done to reduce the dead-time. It also made them very expensive, especially when the crystals were made very small to optimize the spatial resolution.

In the 1980's a great variety of ideas to provide high detection efficiency and spatial resolution, but at the same time keeping the cost reasonable were published. Most involved ways of putting many more than one crystal on one or more PMTs and suing some coding scheme to identify the crystal. The technique which survived was the "block detector" first described by Casey and Nutt[3].

Block detectors are made by cutting deep channels into a solid crystal, and then filling these channels to prevent the light spreading from one section to the next.

All present PET scanners for human use employ scintillation crystals coupled to photomultipliers as their detectors. The first PET scanners [1, 2, 4] used NaI crystals, the same material used in gamma cameras. However most dedicated PET scanners use much denser crystals, and for over 20 years bismuth germanate [5, 6, 7] (commonly referred to as BGO, although its chemical formula is $Bi_4Ge_3O_{12}$) has been the scintillator of choice due its very high density and atomic number. Many other scintillators have been used proposed and some of them used in PET scanners during that time. The most well known are barium fluoride [8], and gadolinium oxy-orthosilicate [9]. The ideal scintillator would be very dense and convert most of the gamma rays energy into light. At the time of writing, the best one is cerium doped lutetium

oxyorthoscilicate [10], commonly known as LSO. This is now used in the latest high performance PET scanners [11].

The important properties of these crystals for PET are given in Table II. The combination of high light output, and short time constant allow for very fast timing which reduce the chance of random coincidences, and reduce the dead time. They also enhance the crystal identification when these crystals are used in block detectors.

| Property / Scintillator | | NaI(Tl) | BGO | LSO |
|---|---|---|---|---|
| Relative light output | | 100 | 15 | 75 |
| Decay constant (nsec) | | 230 | 300 | 40 |
| Density (g/cc) | | 3.67 | 7.13 | 7.40 |
| Effective atomic number | | 51 | 75 | 66 |
| Singles efficiency at 511 keV | 10 mm thick | 29% | 62% | 58% |
| | 25 mm thick | 58% | 91% | 89% |
| Coincidence efficiency at 511 keV | 10 mm thick | 8.4% | 38.4% | 43.6% |
| | 25 mm thick | 33.6% | 82.8% | 79.2% |
| Singles efficiency at 133 keV | 10 mm thick | 93% | 100% | 100% |

**Table II** Properties of commonly used scintillators in PET

The efficiencies given in Table II provide an important insight into the effect of the scintillator material and its stopping power. This singles efficiency for 133 keV photons in a 10 mm thick NaI crystal is 93%, whereas the coincidence efficiency for the same crystal is only 8.4%, making it a very poor choice for PET imaging even though it is excellent for

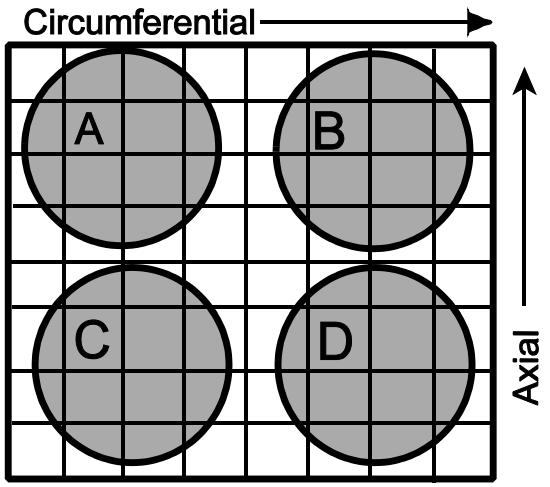


**Figure 5** Crystals and round PMTs in CTI ECAT Exact HR+ PET scanner detector block. (8 x 8 crystals, Overall dimensions: 38 x 36 x 30 mm).

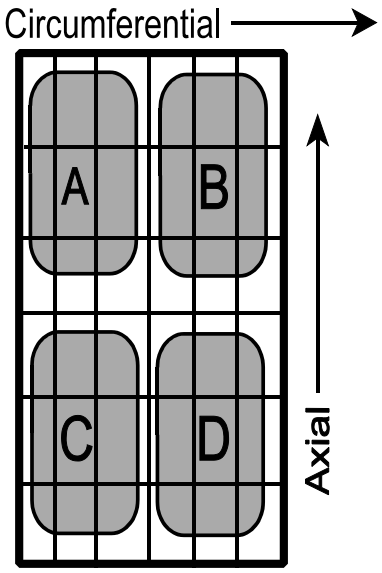


**Figure 6** Crystals and PMTs in GE Advance PET scanner detector block. (6 x 6 crystals. Overall dimensions 26 x 51 x 30 mm)

SPECT with $^{99m}$Tc. On the other hand, 25 mm of BGO or LSO provides about 80% coincident detection for 511 keV, making these crystals superior for PET imaging. Thicker NaI crystals (25mm) are used successfully in PET imaging, although their detection efficiency is about 40% of that from BGO crystals in the same physical geometry.

In most dedicated PET scanners, each detector is a separate module which can be replaced when required. The complete module contains either four PMTs or two dual PMTs, as well as the cut-block scintillation crystal, but no active electronic components, all housed in a light-tight thin metal enclosure. The enclosure provides electrical and magnetic shielding. The BGO crystal dimensions are about 40 x 40 x 30 mm and this is cut into between 6 x 8 to 8 x 8 individual crystals. Diagrams of the crystals and the PMTs for two popular PET scanners is shown in Figures 5, and 6.

**2.3 Signal processing electronics**

Each PET block detector has signal cables for each PMT and requires one high voltage (1600-1800 Volts)connection for the whole module. The signals from each PMT are amplified and filtered, then summed to provide a signal proportional to the energy from which the arrival time of the γ-ray is determined. The time this signal triggers a constant fraction discriminator is measured with respect to a very fast system-wide clock which records the time to the nearest one or 2 nsec. The PMT signals are combined in a way similar to the signals from the PMTs on a gamma camera which is commonly referred to "Anger logic", in honour of Hal Anger the inventor of the gamma camera. With the PMTs referred to as A, B, C, and D the following equations allow an initial position estimate of the incoming γ-rays:

$$X' \frac{[B\&A]\%[D\&C]}{A\%B\%C\%D}$$
$$Y' \frac{[C\&A]\%[D\&B]}{A\%B\%C\%D} \qquad (2)$$
$$E' [A\%B\%C\%D]$$

These three signals can be digitized with eight bit analog to digital converters. If the four signal outputs are properly balanced, a crystal identification pattern like that shown in Figure 7 is obtained. The signal processing module is able to adjust the gains of the individual signals, and make it look like that shown in Figure 7. The dots in this figure show the peak signal surrounded by the territory associated with each crystal element. The X and Y values, from equation 1, are used to address a small memory (on the signal processing module) which provides the crystal address. The sum, or energy, signal is scaled with factor for that crystal, and compared with lower and upper discriminator settings to determine if that γ-ray has an acceptable energy. If it does, the crystal address, and the arrival time of the γ-ray are sent to the coincidence circuit. The crystal address includes the ring number, and the crystal position in the ring. Other information, like the energy window, may also be included in the identification.

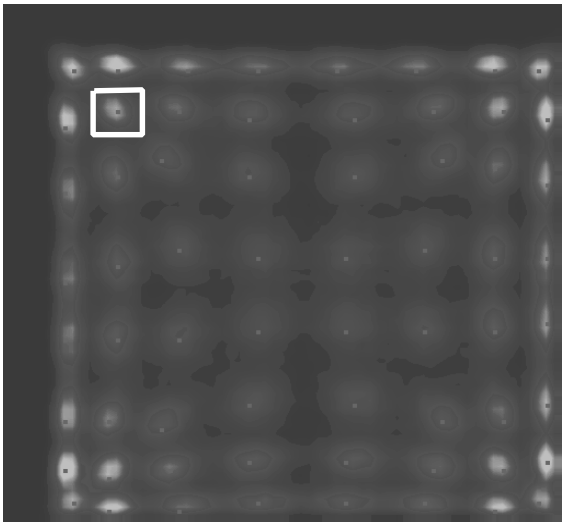

**Figure 7** Crystal identification pattern for a CTI HR+ 8 x 8 crystal block with the territory of one crystal element mapped out (shown in white).

### 2.4 Coincidence circuit

In older scanners analog coincidence circuits were used, but now there are so many crystals, it would be very difficult to do this. Instead the time-stamps from the detector modules are compared, and accepted as coincident when they are equal or nearly equal. The allowable time difference is called the coincidence resolving time and given the symbol $\tau$.

The time-stamps from $\gamma$-ray pairs which are different by a small fixed time are also compared. These would not be in coincidence since the time is too big for that to be so. However these events are representative of the random coincidences, and are used to estimate how many random coincidences there are.

### 2.5 Data acquisition computer

Most modern PET scanners have a separate data acquisition computer system (ACS) from the workstation with which the user sets up, controls and displays the scans. The ACS is comparatively simple as far as functions go, but it requires very large random access memory and disks. Some idea of the size requirements can be appreciated by considering that a PET scanner with a 15 cm field of view divided into D (=24 for the GE Advance") or (=32 for CTI ECAT HR+) crystals deep and 288 detectors in each ring requires (32 x 32 x 288 x 288)/4 (>21 million) memory locations which may receive counts during the acquisition of one image. If this is a gated study 16 times more memory is required. Twice as much memory is needed for dual energy or simultaneous emission/transmission scan. While a typical static PET scan may take about 10 minutes, some dynamic scans have frame times of only a few seconds, and may be as long as 30 frames (>600 MBytes of memory required).

Usually some form of compaction is done, like combining two or four adjacent bins into one when short frame times are used. However, while acquiring any one frame of an image, all of this memory must be available. We can contrast this to a SPECT scanner where one projection angle is acquired at a time, so typically only 128 x 128 (ie 16384) memory locations are required to acquire the counts at any camera angle. Typically a PET scanner requires 1000 times more memory during a scan than a SPECT scanner, even though the size of the final reconstructed image matrix ~(128 x 128 x 64) is about the same.

### 2.6 Reconstruction, display and image analysis systems

Most common PET scanners use separate systems for image reconstruction, display and image analysis. Reconstructing PET images, especially 3D ones is a very compute intensive task, and this is usually handled by special purpose computers called "array processors". These have many small processors which work in parallel all doing the same task, but each working on different parts of the image in order to reconstruct it in a timely way. These require access to the raw data in the ACS memory. Image reconstruction is discussed elsewhere. During the process the reconstructor must access not only the data acquired during the emission scan, it requires data from a normalization scan to calibrate the detector-pair efficiencies, as well as a blank and transmission scan data in order to correct for attenuation, and scattered radiation. Each of these data sets is very large.

An image display facility must be available to the scanner operator in order to verify that the images are technically satisfactory. Most other imaging modalities produce images much faster than PET scanners. (Ultrasound scanners produce real-time images, SPECT scanners can show each projection as it is acquiring, and X-ray CT scanners can now reconstruct images in a few seconds). Since PET deals which much more input data, PET scans are usually reconstructed asynchronously and are not normally displayed as they are reconstructed. One possible reason for this is that the 3D reconstructions process the whole volume at once, so it is only at the end of the process that all images become available at once. Another reason is perhaps that until recently PET was used more for research than clinically on a fee for service basis. The increased used PET as a clinical tool is likely to create a need for faster image

reconstruction, and more accessible images of recent scans.

Off line viewing facilities are almost as necessary as a quick display on the operator's console. PET scanning software now provides for the export of images to nearby workstations, and centralized viewing facilities.

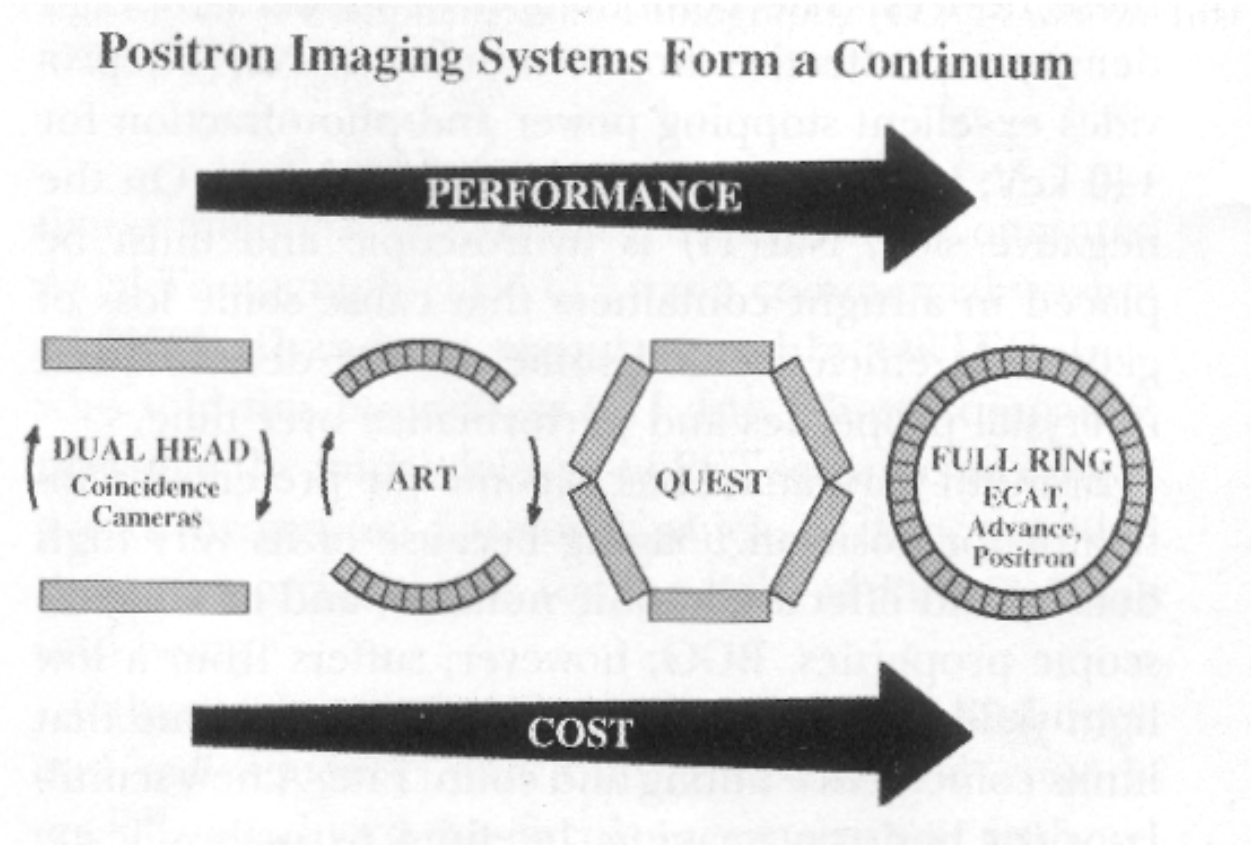


**Figure 8** Available geometries for PET detectors. The first two require rotation of the detectors to acquire all projections needed to form and image. (Reproduced from Phelps and Cherry)

**3 PET detector and collimator configurations**

Since the early 1970's when PET started, there have been three basic detector configurations: Rings of discrete detectors[1, 2], two planar areal detectors[4], and polygons[12, 13] (hexagons and octagons). The vast majority of dedicated PET systems today are in the ring configuration. The discussion so far in this chapter has assumed this configuration. If a scanner is to be used for PET and SPECT, this is not the configuration of choice, even though it is probably the best for dedicated PET systems. An overview of the history of PET geometries and their relative sensitivities by Phelps and Cherry gives some valuable insight

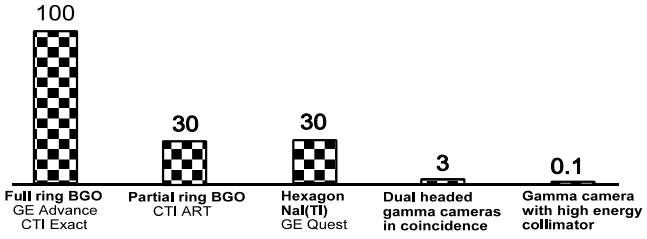


**Figure 9** Relative efficiencies of different PET detector configurations. (Based on Phelps and Cherry)

into the sensitivity and cost of various systems [14]. Figure 8, showing a cost comparison, and figure 9 showing the comparative sensitivities are reproduced from this article.

### 3.1 Ring of scintillation crystals with "Block" detectors

The most common dedicated PET detector systems today consists of individual detector modules in which an array or cut-block of BGO scintillation crystals are coupled to four PMTs as discussed previously. Two of these modules from the Siemens CTI ECAT Exact HR+, and the GE "Advance" are shown as figures 5 and 6. These have several advantages. 1) Each detector is a small independent system. The probability of two γ-rays interacting with a small detector during the scintillator's decay time is obviously smaller than with a larger detector, so the dead time of the individual detectors is very small, so the system dead time is small. 2) Each detector is a light-tight field replaceable module often with only one connector. This reduces the time to repair to that of replacing a faulty module, so improves the availability of the scanner. 3) There is the symmetry which comes with a ring design which provides uniform sampling at all angles.

A disadvantage of this design arises due to the great depth of the crystals required to detect 511 keV γ-rays efficiently. When one attempts to improve the spatial resolution by making the crystals very thin, but retain efficiency by making them long, near the edge for the imaging field the γ-rays may not be detected in the first crystal they enter, but pass through one or two crystals. This effect, referred to as "radial blurring" is characteristic of ring systems, and results in a point source near the edge of the image field appearing in the image as an ellipse which has its major axis along the radius of the scanner. The cause of this effect is illustrated in Figure 10.

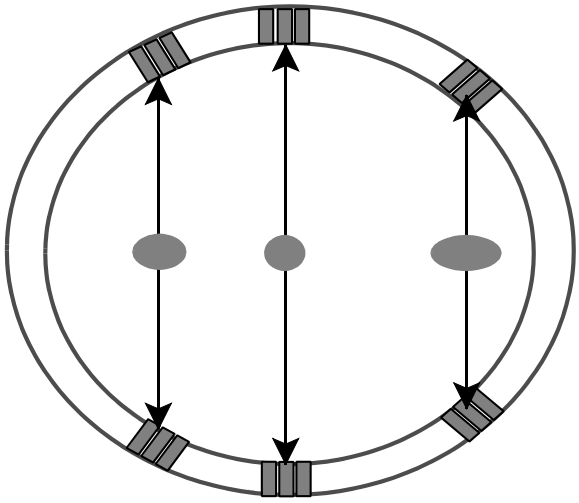

**Figure 10** Radial blurring is caused when the PET crystals are very deep compared with their width. γ-rays from objects near the edge of the field of view may penetrate one of more crystals before being detected. The uncertainty of the crystal in which they are detected causes the image to be blurred radially.

### 3.2 Planar detectors

The very first PET scanners had planar detectors[4], but until quite recently these went out of fashion. The loss of interest in this configuration was mainly due to its dead time. The most common configuration for planar detectors is the conventional gamma camera with a thicker than normal crystal. Using typical "Anger-logic" readout, a gamma camera can only handle one γ-ray at a time. Since, as was shown in the section on "electronic collimation" there are far more unpaired than paired γ-rays detected, and both cause equal dead times, the coincident count rates in these systems is very limited. Modern gamma cameras use individual ADCs for each PMT and the computation of the point of incidence is done digitally. The advantage is that only PMTs in the region of the peak signal intensity are used to compute the position. If two γ-rays strike the crystal face at the same time, but at some distance apart, each is processed separately. This has the effect of reducing the effective area of the gamma as far as dead time is concerned to about 1/10 of the total size.

Another detector configuration which was in vogue before ring systems became dominant, was the hexagonal or octagonal configuration. The PETT IV and early ECAT systems are examples of this

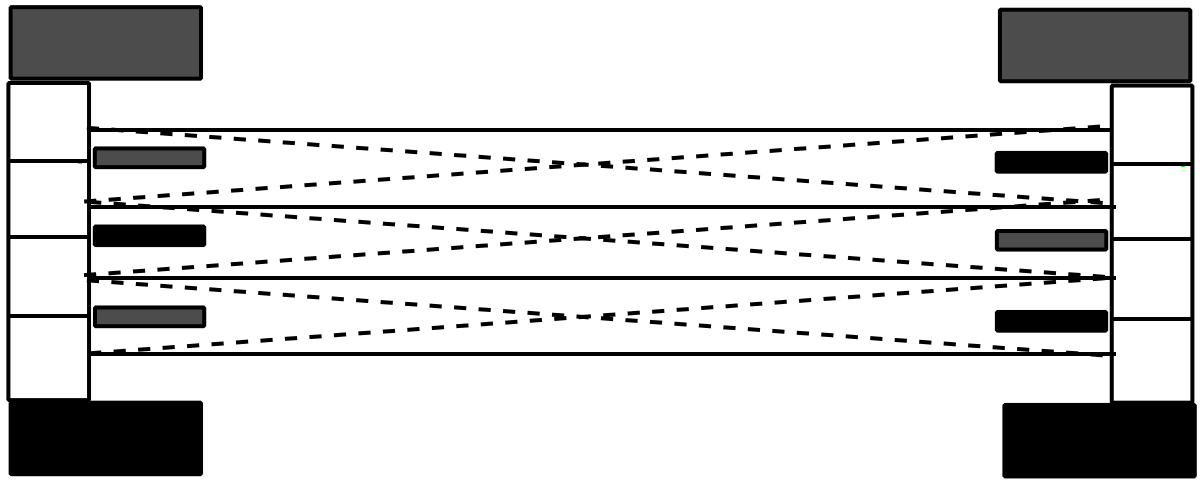

**Figure 11** Multi-slice PET scanner with septa configured for 2D imaging with both direct (solid) and cross (dashed) slices.

configuration. In order to provide adequate sampling, these systems had to rotate and in some cases the detectors also moved along their peripheral direction making them mechanically quite complex. The recent "panel detectors" used by CTI in their high resolution research tomograph (HRRT) represent a revival of this concept [12]. This new system features a dual layer scintillator to minimize radial blurring, and interpolation in the dead zones where the panels join. This allows the detectors to remain stationary.

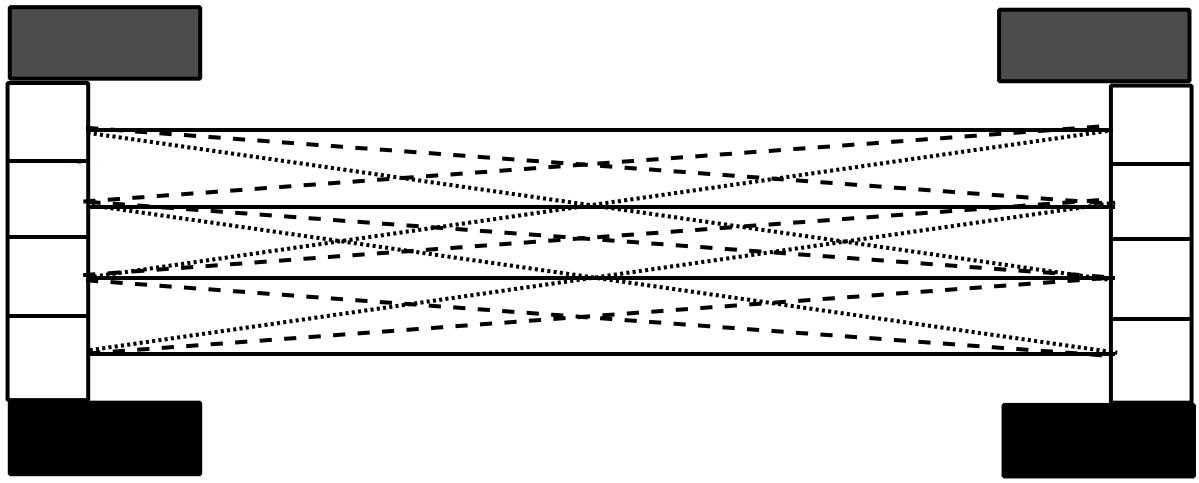

**Figure 12** A PET without septa scanner configured for 3D imaging can accept direct (solid), cross (dashed), and oblique (dotted) slices.

### 3.3 PET emission imaging modes

Many recent PET scanners have septa which are inserted for some studies and retracted for others. These allow the scanner to perform both 2D (Figure 11) and 3D (Figure 12) imaging. While each has advantages and disadvantages, there is a trend towards 3D imaging.

### 3.4 2D PET imaging

2D imaging is performed by positioning thin lead or tungsten annuli (called septa) between adjacent rings of crystals illustrated in Figure 11. The outer diameter of the septa is just less than the inner

diameter of the detector ring. The inner diameter is just wider than the patient scanning aperture. This divides the axial field into clearly delimited planes. γ-rays approaching the detectors from beyond its plane must either travel through many septa (if they originate far from that slice), or very obliquely through one or two septa. In either case, the path length through the lead is long even though the each septum is only one or two mm thick.

2D images are formed as direct or cross slices (Figure 11). The thinnest slices are obtained when only γ-rays which interact with crystals in the same ring are accepted. These are called "direct slices" as opposed to cross slices in which the γ-rays interact with detectors in adjacent rings. The direct slices are slightly thinner than the cross slices especially near the edge of the field of view. The sensitivity of the scanner can be improved at the expense of axial resolution, by allowing the direct slices to be augmented from the addition of events whose γ-rays come from crystals which are two rings apart, and the cross slices made from crystals which are three rings apart.

2D images are quite well defined, and contain very little contamination from events outside their axial extent. In this mode the scanner is relatively insensitive to scattered radiation from within the plane since, in order to reach a detector, a γ-ray would probably have to scatter twice, or be scattered through a very small angle to be detected in the same plane. Until recently, 2D imaging was considered most quantitative than 3D imaging, but more accurate, and faster 3D scatter correction algorithms are now available, so the trend is towards 3D imaging for all emission scans.

### 3.5 3D PET imaging

The septa in newer PET scanners can be retracted exposing the detectors to oblique as well as trans-axial γ-ray pairs as shown in figure 12. This increases the efficiency to unscattered rays by about five times depending on the range of oblique angles accepted. At the same time the sensitivity to scattered rays goes up by about 20 times, so scatter fractions are much higher in 3D than 2D imaging. In most cases the additional scattered rays have scattered only once in 3D imaging, so correction algorithms based on single rather than multiple scattering can be used and do very well in correcting the image for the loss of contrast due to the detection of scattered radiation.

PET scanners with planar detectors do not have septa, so always work in the 3D mode.

## 4 Attenuation correction and transmission scans

PET is considered as a quantitative imaging technique, so that the images can be calibrated in units of activity concentration (kBq/ml, or nCi/ml). In order for this to be true the images must be corrected for the effects of attenuation. The 511 keV γ-rays in PET have greater penetration in body tissue than the 133 keV γ-rays from $^{99m}$Tc, however both rays must emerge and be detected in PET whereas only is recorded in single photon imaging. An important distinction between PET and SPECT is that in PET the measurement of attenuation can be made completely independently of the isotope distribution. This is illustrated in figure 13. A positron annihilating a the point represented by the black dot produces two γ-rays one of which travels $d_1$, and the other $d_2$. The probability of each of them emerging is $e^{-\mu d_1}$ and $e^{-\mu d_2}$, but the probability of both them emerging is the product of the probabilities, or, as shown in equation 2: $e^{-\mu D}$.

$$\begin{aligned} A_1 &= e^{-\mu d_1} \\ A_2 &= e^{-\mu d_2} \\ A_1 \cdot A_2 &= e^{-\mu(d_1 + d_2)} \\ A &= e^{-\mu D} \end{aligned} \qquad (3)$$

The importance of this is that the attenuation along a particular line of response is independent of the point where the positron annihilates. In fact, a simple extension of equation 3 to a case non-uniform attenuation can be made, ie where μ varies along the path, and the γ-ray encounters fat, lung, and bone on its path towards the detector.

$$A' e^{-\int_{path} \mu(l)\, dl} \qquad (4)$$

Figure 14 shows an isolated point of activity, which is outside the body section. Even though it is outside the body, equation 3 still applies, and this is used to make an independent measurement of the attenuation is the section being imaged. This type of image is called a transmission scan. The primary purpose of this procedure is for attenuation correction, but the data can also be used to make anatomical images if it collected is processed correctly.

Transmission scans are acquired with one or more orbiting external sources as shown previously. In order to form and image, or provide data for attenuation correction, the number of events in each bin of the transmission scan's sinogram, T(r, β), are divided into the number of events obtained during the equivalent time during a blank scan, B(r, β) (ie with nothing in the scan field). A "ratio" sinogram is produced, R(r, β), and this is used to correct the emission counts in each bin while reconstructing the emission scan. If the natural logarithm of this ratio is taken, and the resulting attenuation sinogram A(r, β) reconstructed, an attenuation image is produced.

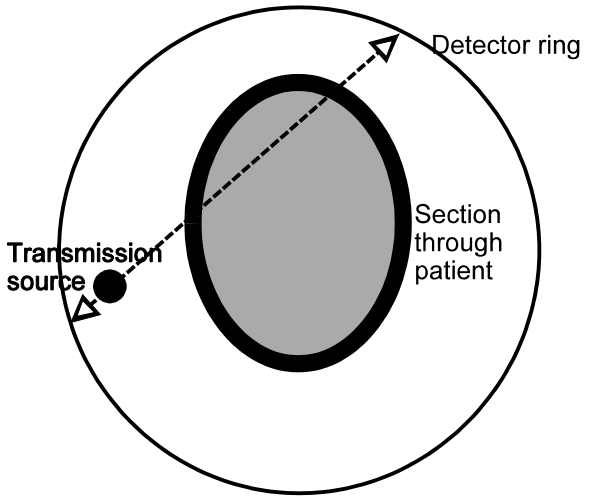


**Figure 13** The transmission is source outside object to be scanned. Since the attenuation along any line is independent of the source position, the attenuation in a body section can be measured using an external source.

$$R(r,\beta) = \frac{B(r,\beta)}{T(r,\beta)}$$
$$A(r,\beta) = \ln\left(\frac{B(r,\beta)}{T(r,\beta)}\right) \qquad (5)$$

An image which resembles a low contrast X-ray CT scan is obtained. The contrast is lower since the range of variation in tissue attenuation at high energies is lower at higher energies. These are very useful in identifying the anatomical regions, especially if they are compared feature for feature with CT or MRI images, since they map the tissue density, not function.

### 4.1 Rod sources

The fact that the attenuation for the pair of γ-rays is independent of the location of the positron is used very effectively in the most common technique for measuring attenuation. One or three thin rods of $^{68}$Ge are introduced as close as practical to the inner surface of the septa and collimators. During a transmission scan, these sources orbit the scan field just outside the tunnel through which the patient is imaged. During a transmission scan only pairs of detectors which are collinear with the current location of the source are enabled to store counts. The fact that these scans are done with the septa in place, and that the source and detectors are collinear prevents almost all scattered radiation being detected, and provides a very accurate measurement of the attenuation along all lines of response.

The main advantage of this method is its potential accuracy. The main limitation is due to the very high count-rate which is received by detectors which are near the current source position. In order to obtain sufficient counts for a good quality transmission scan, one must either count at a high rate, or for a long time. The former imposes an upper limit due to dead time and pulse pile-up in the detectors near the source, and the later makes for longer scanning times.

### 4.2 $^{137}$Cs point sources

In order to improve the counting statistics in transmission scans, some scanners now use one or more point sources of $^{137}$Cs. This isotope has a 662 keV γ-ray and it is available with very high specific activity so very concentrated small point sources can be made. The point source orbits the scan field in a spiral fashion, and the line joining the distant detector, and the current point source is extrapolated to the point where it intersects the near detector surface. This identifies a dummy detector with which the second γ-ray would have interacted, had the source been a positron rather than a single gamma emitter. This is accomplished using real-time electronics which uses look-up tables to perform the calculations.

The main advantage of this method is the lack of dead time in the near detector which allows for much stronger sources, and faster scans. The disadvantage is the lack of a collinearity condition allows much more scattered radiation to be detected. Since this technique is commonly used with 3D scanning, the scatter fraction in these scans is very high, so the contrast is lower. The higher primary energy of the γ-ray also reduces the contrast, so the final scan is often segmented into zone corresponding to soft tissue, bones and lung-tissue, and the appropriate values for the attenuation at 511 keV are then associated with each region.

### 4.3 Use of images from CT or MRI for attenuation correction

Another technique which can be used for attenuation correction is to import cross-sectional images of the same body sections from CT or MRI. To make this work, the tissue must be segmented based on the contrast mechanism in MRI or attenuation at much lower energies in the case of CT images, and each pixel assigned an appropriate attenuation coefficient at 511 keV. Image registration is a significant problem with this technique. The couches of both PET and CT scanners will probably be a different shape, and the patient will probably be positioned differently, making this a serious problem. Recently PET-CT scanners have been introduced to overcome this problem, but these represent a rather expensive solution to this problem.

### 4.4 Post-injection attenuation scans

The previous sections assume that there is no radioactivity in the patient. If there is, it will be detected along with that from the external source, and this will reduce the contrast, (and by implication) the attenuation values obtained during the transmission scan. When several bed positions are required to investigate a large axial extent of the patient, it would be necessary to have the patient scanned twice once for the attenuation measurement, and then have a tracer injection followed by and uptake period of about 40 minutes, and the emission scan. This requires a very long scan time. It is unrealistically long for the

patient, and severely impacts the number of patients who could be scanned a day.

### 4.5 Simultaneous emission/transmission scans

Using the collinearity condition set up by the location of the rods, we have shown that an attenuation scan which is free from contamination can be obtained. But what about detector pairs which are nowhere near collinear with the rod position. These can still record counts from the radioactivity injected in the patient. This allows the possibility of simultaneous emission/transmission scans. Here there are two sinograms for each patient section. High speed electronics (mostly look up tables) determine, on an event by event basis, if the line joining the two detectors is, or is not collinear with the current position of the source. The yes/no result decides whether the event is considered an emission or transmission count, and the appropriate bin of the correct sinogram is incremented.

## 5 Sources of noise in PET images

All medical imaging techniques are limited by signal to noise considerations. In most cases, image quality improves with longer measurement time to provide more photons. PET is no exception to this, and there are more sources of noise in PET images than in conventional Nuclear Medicine single photon imaging.

### 5.1 Poisson counting noise

All nuclear medicine techniques involve "counting photons". These photons are emitted from the body, as distinct from X-ray imaging which measures (but rarely actually counts) the photons which are not absorbed by the body. To minimize the radiation dose, only enough tracer is injected form a useful image, since all organs are exposed to the injected radiation, whereas the external X-ray beam is collimated to match the detector area. After the tracer is injected, the patient is exposed to its radiation for a long time compared to the scanning time, whereas, he is only exposed while the X-ray beam is on. So for an equivalent radiation dose, far more X-ray photons will be absorbed by the detector than during the acquisition of a Nuclear Medicine image.

In the case of a digitally acquired planar gamma camera image, the number of counts in each pixel is directly proportional to the pixel area and the effective counting time (ie the decay-corrected counting time). Since radioactive decay is a random process, the number of counts acquired in two measurements will not be the same. In fact, the number of counts, N, acquired per unit time has an uncertainty such that the standard deviation is %N. Images acquired with short times have far more noise expressed as a percentage of the mean counts (ie 100*%N/N, or 100*%N). For the same reason images divided into more smaller pixels show more noise.

The propagation of noise into a reconstructed image from projections is outside the scope of this section, but the noise does propagate, and the more noise in the projections, the more noise in the final image.

### 5.2 Scattered counts

When $\gamma$-rays are scattered before reaching the detector, the LOR joining the two detectors no longer passes through the point of annihilation, resulting in a loss of contrast. The contrast can be restored by making an estimate of the scattered counts in each LOR and subtracting it from the observed counts. The estimate is often made by convolving each projection (horizontal line in a sinogram) with a smoothing function which is characteristic of the scattering probability in that projection. When this is done the scatter-profile is a smooth function which extends beyond the true-count profile. When this is subtracted the resulting total-scatter projection will have the same total noise than previously, however since something is subtracted, the percentage noise will increase, since $100*\%N/(N-S) > 100*\%N/(N)$.

### 5.3 Random counts

Random counts are unique to PET imaging and represent an additional source of noise which must be estimated and removed in order to prevent a loss of image contrast. Random counts arise when two γ-rays from different annihilations strike two detectors nearly simultaneously. As discussed previously, each detector records many single counts for each coincident count. When there is a lot of activity, it is very likely that two of these single counts will occur within the time window τ during which two detected γ-rays are considered simultaneous. If two crystals have single γ-ray countrates of $S_1$ and $S_2$, then the random countrate, R, for these detectors will be:

$$R = 2\tau S_1 S_2 \qquad (6)$$

In order to correct for random counts, the countrate is first estimated, then subtracted in each point in the sinogram. The most common way of doing this is to use two timing windows, one for prompt counts, and another which is delayed by a few tens of nanoseconds. In this window, a true coincidence (ie one arising from the same annihilation) is impossible, but a random coincidence is just as likely to occur, as it would be in the normal timing window.

There is an uncertainty associated with making this measurement so this is an additional source of noise. If R is the random coincidence rate, the percentage noise in this measurement is 100*%R/R. To obtain the true count rate associated with any LOR, we must use the measured count rate, N, less the scattered, S, and random, R, count rates, so:

$$T = N - S - R \qquad (7)$$

### 5.4 Dead time

As stated previously, the electronic collimation used in PET requires that all γ-rays which interact with the detector be initially processed, and then probably discarded when they are found not to be in coincidence. Each detector can only record one γ-ray at a time. If another interacts with the detector while it is still scintillating after the last one, both the energy and position of both γ-rays will be wrong, and the timing signal from the second one will be lost. Since the PMT signals are filtered in order to measure their values more precisely, the minimum time to process each interaction is about 1000 nsec. for BGO crystals, and about 200 nsec for LSO and NaI crystals which are both faster and emit more light. While this may not seem like a very long time, if the singles count rate in a crystal is a few hundred thousand counts per second, it will be unable to respond much of the time. This time during which it is unavailable is called the "dead time". It depends on the total count rate on each detector. Making the detectors smaller reduces their countrates, and this is a major consideration in PET detector design. The area of a gamma camera crystal is many times that of a PET detector, although the newer gamma cameras can process more than one incident γ-ray at a time if they interact with the crystals sufficiently far apart.

### 5.5 The concept of noise-effective counts

The noise due to counting photons is only part of the story in PET images, since there are both true unscattered photon pairs detected, which are the only source of signal, and are subject to normal Poisson counting statistical noise, but there are also scattered and random counts which contribute no signal, only noise to the image. The noise in PET images is worse than it would be in a simple planar counting study for a given number of true counts recorded, but there would be many more true counts detected for a given activity concentration than there would be in a conventional gamma camera image.

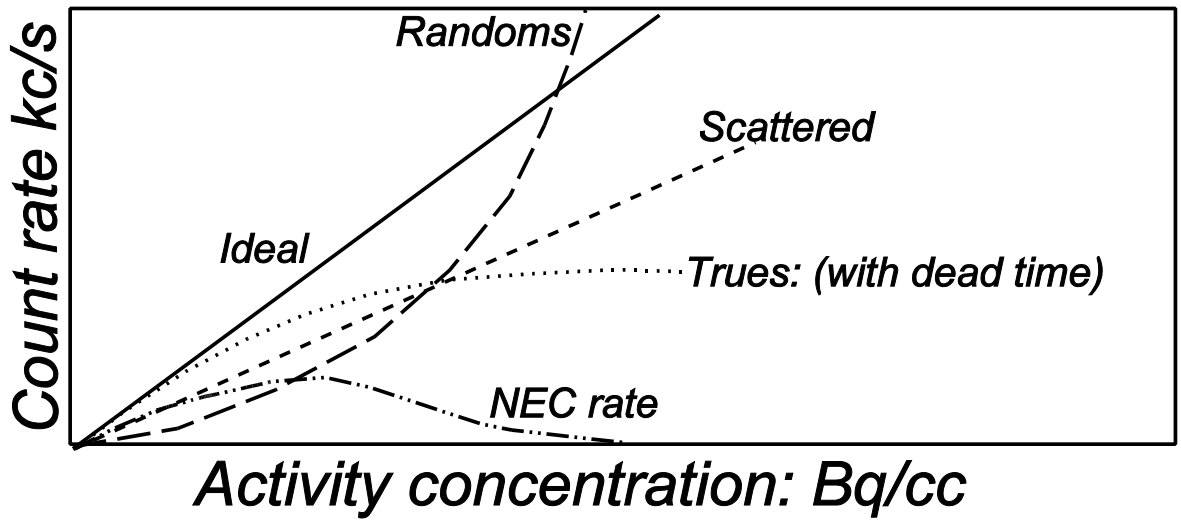


**Figure 14** An ideal PET scanner with no dead time would have a count-rate directly proportional to the activity concentration. The scattered counts are a constant fraction of the true counts, whereas the random count-rate increases with the square of the activity concentration. Dead time limits the efficiency as the activity concentration increases. The noise-effective count-rate (NEC) first rises then plateaus and eventually falls.

One can think of the true PET counts being "devalued" due to the corrections for random and scattered counts. This concept is referred as a noise-effective count rate. It is the equivalent rate for true counts had the other sources of noise not been present. If N is the coincidence count rate, T is the true count rate, S is the scattered count rate, and R is the random count rate, then:

$$NEC = \frac{T}{1 + \frac{S}{T} + \frac{2\tau R}{T}} \qquad (8)$$

The terms S/T and R/T (which are always positive) serve to reduce the effective counting rate. The scatter fraction S/T is constant for a given imaging situation, but the random rate increases as the activity and count rate increases. The NEC is depicted in figure 15 along with the ideal performance of a scanner, and the trues, randoms, and scattered count rates. So at high activity concentrations, serves to limit the NEC, so that the NEC actually falls if the activity concentration is increased. An analogy can be made with the scatter fraction S/T is like the sales (or value-added) tax on and article in a shop, which is the same for everyone. The random fraction R/T however, increases like income tax, so the more you earn, proportionally the more you pay!

**5.6 Out-of-field counts**

The scanner can only detect true counts from within its filed of view. However activity outside the field can contribute large numbers of single γ-rays which will contribute to the random counts, and also scattered counts. The septa used in 2D imaging are quite effective at attenuating out-of-field counts, but 3D studies are much more prone to contamination due to out of field counts. This is especially problematic with dual headed coincidence cameras, which are poorly shielded against out-of field events.

### 5.7 Noise from attenuation correction

In order to obtain quantitative PET images, one must correct for attenuation. Failure to do so results in an over estimation of the activity concentration at the edge of the body section, and an artificially high activity concentration observed in low density tissue regions like the lungs. There has been a significant debate in recent PET literature on whether to do attenuation correction at all if all one needs is to "see" a hot spot. Attenuation correction using transmission scans takes time and adds noise to the emission image. Does it add diagnostic value? This question will be addressed elsewhere...

Since the attenuation correction or image from a transmission is the result of dividing the data in the blank scan's bins by the data in the transmission scan's bins, the noise in the attenuation correction map or image is very different. LORs containing more activity have higher counts and thus lower noise in an emission scan. However if a LOR parses through a region of high attenuation it will have lower counts in the transmission scan. Since each bin is divided into a blank scan bin, the resulting bin will contain bigger number. Thus the noise in regions of higher attenuation is higher than in regions of lower attenuation. If the transmission is acquired for a short time on an obese patient, it is possible that some sinogram bins will contain no counts at all! This would result in dividing by zero.

Some pre-processing of the transmission scan data is always done, including interpolation of all zero and negative bins and smoothing the transmission sinogram before dividing it into the blank scan.

Often some post processing in the form of image segmentation is performed. The basis of this comes from the observation that there are really only four likely values of attenuation coefficient in PET imaging, those for air, lung tissue, water equivalent tissue, and bone. Boundary finding and artefact detecting algorithms are applied to catagorize each region in the attenuation image, and the most probable value assigned to each region. When properly applied these can eliminate the noise from transmission scans thus permitting quantitative imaging in a timely fashion.

## 6 PET imaging modes

### 6.1 Static emission scans

A static PET image is one made during a period when the activity distribution is fairly stable, and the counting time is long enough to obtain a good quality image. Typical applications are in the measurement of the glucose metabolism of the brain or heart using the tracer FDG. The half-life is long, and the whole brain or heart can be imaged in one scan if the axial scan field is about 15 cm. Another example is in cerebral blood flow "activation" studies with $^{15}$O-water. If the scan is started about 15 seconds after injection and lasts one minute, the scan captures a fairly constant count rate at the peak of the activity concentration in the brain. In both these cases a model exists to derive the functional parameter (glucose utilization of blood flow) from a single image.

### 6.2 Dynamic emission scans

Dynamic studies are used in cases where it is necessary to follow the activity over a long period in order apply a more complex model of the underlying physiology. This is done to extract several rate constants for the biological process. Oxygen consumption measurement, neuro-receptor and neuro-transmitter studies require dynamic scans.

Dynamic scans are performed with the subject stationary, in a series of imaging frames, which normally get longer as the study progresses. Often they are accompanied by either arterial or venous blood sampling in order to provide in "input function" representing the activity concentration of the tracer in the blood during the scanning session. Each image is reconstructed as if it were acquired independently of the others.

The time series of images can be analyzed by placing regions-of-interest or ROIs over important areas in one image, and having a suitable image analysis program provide a time-activity-curve (TAC)

where the activity concentration in Bq/cc is provided as a function of time. This data and the input-function's TAC are input to the model to provide the biological rate constants for each region chosen.

Studies to measure oxygen consumption are often done with 5 -10 second frames over a period of 2 - 3 minutes. Receptor studies take over an hour with the frame time changing from 10 seconds at the start to 5 minutes near the end.

Only one attenuation scan is required and it is used to correct all frames. The subject must remain very still in order that the ROIs chosen on one frame correspond to the same tissue throughout the study, and that the attenuation map remains registered with the correct body section throughout the study.

### 6.3 "Whole body" scans

Whole body scan are the fastest growing application of PET. These studies, which rarely cover the whole body, provide one of the most effective means of looking for tumour metastateses. FDG is the tracer of choice in these both for its good specificity, its long half life and ease of availability. These studies are performed in several "bed positions" by acquiring an emission scan for 5-10 minutes then moving the patient by a distance which is somewhat less that the scanner's axial field of view. Sometimes an emission scan series is done followed by a transmission scan series in the same bed positions. Often, transmission and emission scans are done in an interleaved fashion. The former is subject to mis-registration of the data due to intervening patient movement, the later requires re-configuring the scanner, (acquisition mode, transmission sources, and possibly septa) and can waste a lot of time during the session.

These studies are reconstructed as a series of slices which are saved as a "volume" of perhaps 128 x 128 x 2048 pixels. The volume is then re-sliced horizontally of vertically with respect to the prone patient providing slices through the body in the coronal or sagittal planes. Many examples of these scans are given elsewhere in this book.

## 7 Quality control PET imaging

This section discusses some of the steps taken to ensure that the scanner produces consistently high quality images.

### 7.1 Quantitative imaging vs "making pictures"

When PET scanners are used for producing whole body scans it is the human interpretation of the images in the context of the suspected disease which is the end product of the PET scan. Nuclear Medicine Physicians and Radiologists are used to evaluating "images" as part of their training and with experience can distinguish between an artefact and a region of an image which is suspicious for cancer or and infarct. The most common parameter extracted from these images is the standard uptake value or SUV. This is related to the injected dose/per body mass and is usually higher in tumours than in healthy tissue. In order to make this measurement, and attenuation scan must be preformed and used to correct the emission scan. In the interpretation of these images, the suspicious region is identified visually, and then appropriate software tools provide the SUV in that region.

Other applications of PET in Cardiology or Neurology require dynamic scanning. The estimation of parameters from these scan-sequences is more complex, and requires greater attention to issues related to scanner calibration.

### 7.2 Calibration of individual detectors

The calibration of individual detectors produces a pattern which looks like the one in figure 9. Here the 8 rows and columns of detectors in a CT HR+ block are easily distinguished, and a dot marks the

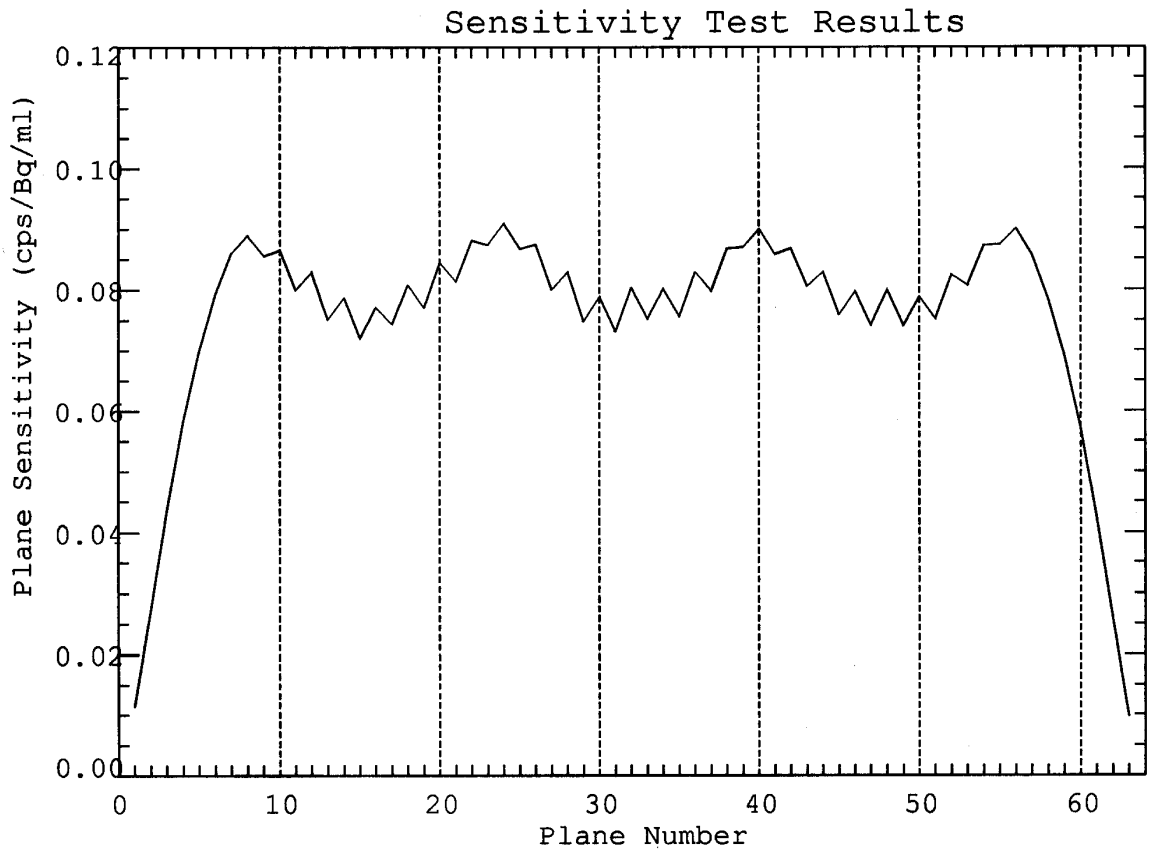


**Figure 15** Plane by plane sensitivity for 63 slices of a CTI ECAT HR+ scanner in the 2D mode tested with a 20 cm diameter NEMA flood phantom filled with $^{68}$Ge plastic resin. The saw-tooth pattern is due to the fact that more detectors contribute to the cross slices than to the direct slices. The four peaks are due to the fact that the crystals in the centre of each block are more efficient than those at the edge.

peak of each crystal's territory in the map. If one PMT is weak the pattern is "pulled away" from it, resulting in a distorted picture. Examination of the individual detector patterns is normally a service function. The detectors must all be working properly before other calibration procedures are performed.

**7.3 Daily blank scans**

As mentioned in the section on attenuation correction, a blank scan (one with nothing in the scan field) is required to estimate the attenuation coefficients for each line of response. This scan is used to correct a lot of studies. To prevent noise in this scan being propagated to all other scans, it makes sense for this scan to be noise-free. Many newer scanners are equipped to do this scan without an operator present. This allows the blank scan to be done for about an hour during the night when it would not be in use.

Examination of this scan will show up faults like a bad detector (which appears as a diagonal band on a sinogram). An automated analysis tool can compare today's blank scan with recent ones, and report changes which indicate that the system requires re-calibration or repair.

During a blank scan the transmission sources are exposed, so the scanner becomes a source of radiation with nobody present. While this seems appropriate for the radiation exposure point of view, it is not a normal procedure with other radiation emitting devices, (eg a radiation therapy machine, of X-ray

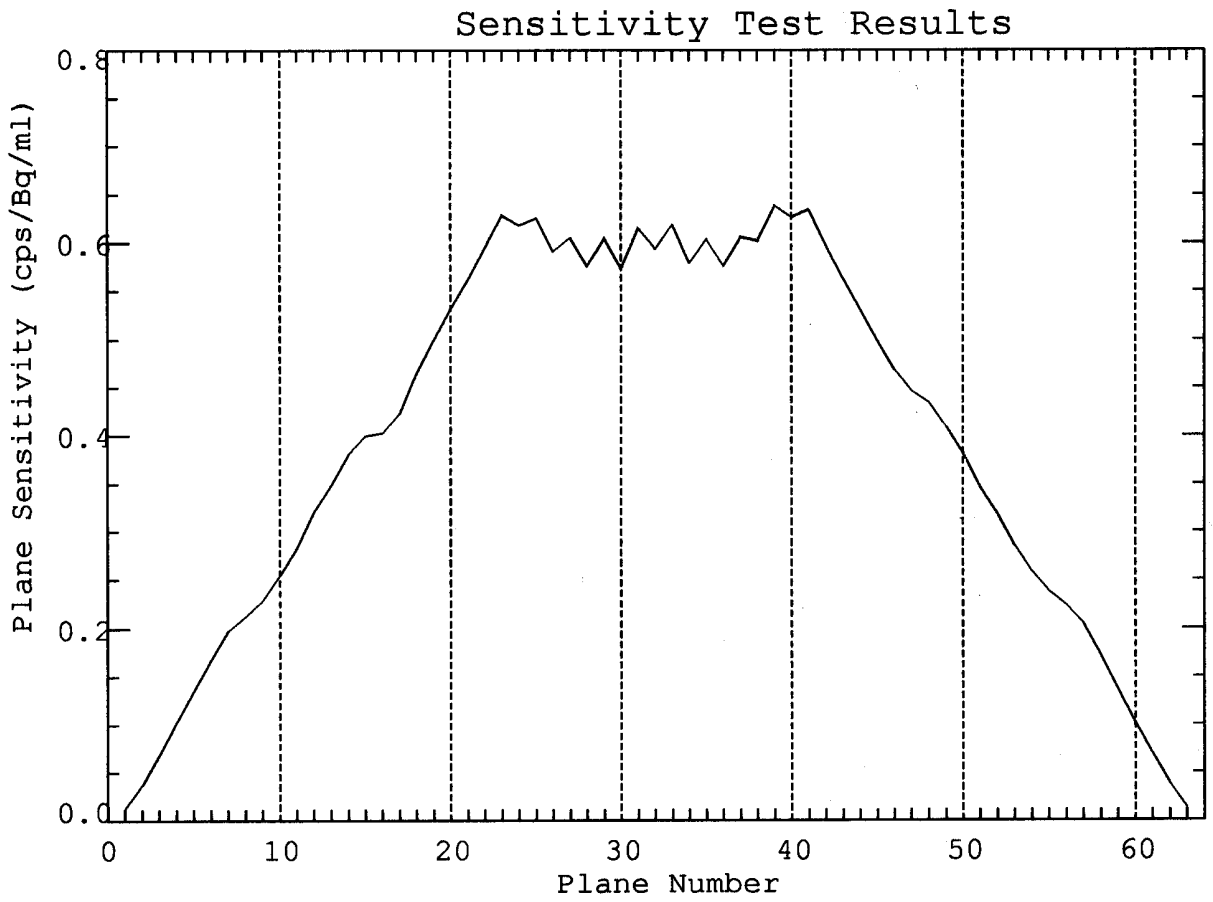


**Figure 16** Plane by plane sensitivity for 63 slices of a CTI ECAT HR+ scanner in the 3D mode tested with a 20 cm diameter NEMA flood phantom filled with $^{68}$Ge plastic resin. Note that the peak sensitivity is about 9 times greater than in the 2D mode. The sensitivity falls off rapidly outside the central 1/3 of the axial field. For this reason there is great value in positioning the organ of interest in the central region.

system which suddenly turned itself on during the night would not be considered safe). Those involved in radiation safety should be alerted to the fact that the PET scanner does this.

### 7.4 Normalization of detector system

The normalization of the lines of response is required to produce uniform images. Some systems require separate normalization for 2D and 3D imaging, so a strong and a weak source are required. Usually a 20 cm diameter source is placed in the centre of the field of view, and counted for a long time. From the size of the source, the length of the chords through it, and the number of counts obtained in each LOR, a calibration factor is obtained for all the LORs which pass through the source. The other LORs are normalized based on the coincidence efficiencies of each detector as measured along the chords which intersect the source.

### 7.5 Calibration of each image plane

If an object of known size, whose activity concentration is known, it is possible to calibrate the individual slices of a PET scanner. This calibration is essential for quantitative imaging, but also very important in the production of whole body scans. The efficiency of each plane can be very different. Even

in 2D imaging the cross planes (odd numbered ones) are more efficient than the direct planes (even numbered ones) as illustrated in figure 16 (for the CTI HR+), since there are more detectors available for cross planes than direct planes. The sensitivity in 3D imaging is very much greater near the axial centre of the field of view due to the contribution of the oblique planes to the central region. Figure 17 shows the sensitivity of the CTI HR+ in the 3D mode. Note the vertical scales on figures 16 and 17 are different by almost a factor of seven. The plane sensitivity numbers, in (counts/second)/(Bq/ml), for each plane as shown in figures 16 and 17 are used as calibration factors during image reconstruction.

### 7.6 Cross Calibration: Isotope calibrator - PET scanner - well counter

Patient doses are usually measured in an isotope calibrator. This instrument is a shielded well-shaped ionization chamber into which a small vial or the syringe containing the patient dose is placed. It is designed for measuring high activities and is unsuitable for measuring blood samples. The PET scanner is calibrated to provide quantitative images in Bq/ml (or nCi/ml). A well counter, used for measuring blood samples is a well shaped NaI crystal connected to a counting system, which normally provides a reading in counts/second.

The suppliers of calibration sources include a small sample of the activity from the calibration source that can fit in the well counter. The activity in the sample, and the date of the measurement is provided by the supplier, so it is possible to calibrate the well counter in Bq/(counts/second) or in "how many atoms decay for each count recorded". An efficient well counter has an efficiency of about 0.4 Bq/(counts/sec) so it can detect 40% of the atoms which decay within the well.

PET scanner efficiencies are usually quoted as (counts/second)/(Bq/ml), as discussed in the previous section. However these are measured from either the entire source volume, to get the total efficiency, or the slice volume as above. To get these in the same units the PET values must be corrected for the slice or total source volume. If the slices are assumed to have the thickness of the crystals (eg 0.4 cm), and the calibration source has a radius of 10 cm the slice volume is 25 $cm^2$ so the plane sensitivity near the centre of a 3D PET scanner is about 0.6 cps/(Bq/ml)/slice volume or 0.024 cps/Bq. Thus the central planes of a PET scanner will detect about 2.4% of the atoms which decay.

A very useful check on the cross calibration of a PET scanner, is to take a typical patient dose and add it to distilled water in a cylinder the same size as is used to calibrate the PET scanner. If the dose is first measured in the isotope calibrator, and a known volume from the diluted solution is measured in the well counter, it is possible to cross calibrate the isotope calibrator, scanner and well counter if the times and dilution factor is recorded.

## 8 Summary

This chapter has provided an overview of PET instrumentation. The basics of positron decay and the subsequent detection of the annihilation radiation have been discussed in sufficient detail to show how the raw data to form PET images is acquired and processed. Questions of sensitivity of different detector and collimator configurations were discussed in the context of their impact on image quality. Different imaging modes were compared and the requirements of each presented. Finally some of the calibration procedures required to produce quantitative images were presented.

## 9 References


1 Robertson J, Marr R, Rosenbaum B: "Thirty-two Crystal Positron Transverse Section Detector" In: Freedman, G Ed: Tomographic Imaging in Nuclear Medicine. New York Society of Nuclear Medicine (1973) 151-153.

2 Derenzo S, Budinger T, Cahoon J, Greenberg J, Huesmann R, and Vuletich T: "The Donner 280 Crystal High Resolution Positron Tomograph" *IEEE Trans. Nucl. Sci.* **NS-26**: 2790-2793 (1979).

3 Casey M E, Nutt R: "A Multicrystal Two Dimensional BGO Detector System for Positron Emission Tomography" *IEEE Trans Nucl Sci* **NS-33**: 460-463 (1986).
4 Anger H: "Multiple Plane Tomographic Scanner" In: Freedman, G Ed: Tomographic Imaging in Nuclear Medicine. New York Society of Nuclear Medicine (1973) 2-15.
5 Weber M J, Monchamp R R: "Luminescence of $Bi_4Ge_3O_{12}$: Spectral and Decay Properties" *J. Appl Phys* **44**: 5495-5499, (1973).
6 Cho Z K, and Farhuki M R: "Bismuth Germanate as a Potential Scintillator in Positron Cameras" *J. Nucl. Med.* **18**: 840-844 (1977).
7 Thompson C J, Yamamoto Y L, Meyer E: "Positome II: A High Efficiency Positron Imaging Device for Dynamic Brain Studies" *IEEE Trans. Nucl. Sci.* **NS-26**: 585-589 (1979).
8 Wong W H, Mullani N A, Wardworth G, Hartz R K: "Characteristics of Small Barium Fluoride ($BaF_2$) Scintillation for High Intrinsic Resolution Time-of-Flight Positron Emission Tomography" *IEEE Trans. Nucl. Sci.* **NS-31**: 381-386 (1984).
9 Takagi K, Fukazawa T: "Cerium-Activated $Gd_2SiO_5$ Single Crystal Scintillator" *Appl. Phys. Lett*. **42**: 43-45 (1983).
10 Melcher C L, Schweitzer J S: "Cerium-doped Lutetium Oxyorthosilicate: A Fast, Efficient, New Scintillator" *IEEE Trans. Nucl. Sci.* **39**: 502-505 (1992).
11 Wienhard K, Scmannd M, Casey M E, et al. "The ECAT HRRT: Performance Evaluation of the New High Resolution Research Tomograph" in: Proceedings of the PET-2000 Ecat Users' Meeting, Barcelona August 2000.
12 Williams C W, Crabtree M C, Burgiss S G: "Design and Performance Characteristics of a Positron Emission Computed Axial Tomograph ECAT-II" *IEEE Trans Nucl Sci* **NS-26**:619-627 (1979).
13 Hoffman E J, Phelps M E, Huang S C:"Performance Evaluation of a Positron Tomograph Designed for Brain Imaging" *J Nucl Med* **24**: 245-257 (1983).
14 Phelps M E, and Cherry S R: "The Changing Design of Positron Imaging Systems" *Clinical Positron Imaging* **1**: 31-45 (1998).